Viscoelasticity in Polymers: Phenomenological to Molecular Mathematical Modelling

H.T. Banks, N.S. Luke and J.R. Samuels, Jr.
Center for Research in Scientific Computation
North Carolina State University
Raleigh, NC 27695-8205

December 14, 2006

Dedicated to Professor Ivo M. Babuska on the occasion of his 80th birthday.

Abstract

We report on two recent advances in the modelling of viscoelastic polymers: (*i*) a new constitutive model which combines the virtual stick-slip continuum "molecular-based" ideas of Johnson and Stacer with the Rouse bead chain ideas; (*ii*) a two-dimensional version of a model that accounts for stenosis-driven shear wave propagation in biotissue.

1 Introduction

The mathematical modelling of *viscoelasticity* (sometimes also loosely referred to as *hysteresis*) in materials using ideas from elasticity has attracted the attention of a large number of investigators over the past century. Among significant contributors (see the many references in [15, 16, 17, 18, 19, 28, 30, 31, 33, 34, 35]) have been some of the true giants from the fields of engineering and material sciences including [1] the distinguished mathematician to whom this paper is dedicated. One of the most widely used empirical models for viscoelasticity in materials is the Boltzmann convolution law [10, 17, 18, 19, 35], one form of which is given in equation (1) below;

for summaries and further references, see Chapter 2 of [19] as well as [10]. This form of model, when incorporated into force balance laws, results in integro-partial differential equations which are most often phenomenological in nature as well as being computationally challenging. One approach to overcome both conceptual and computational challenges is founded on the belief that hysteresis is actually a manifestation of the presence of multiple scales in a physical or biological material system that is frequently modelled (and masked) with a phenomenological representation such as an hysteresis integral for the macroscopic stress-strain constitutive law. A conceptual framework that is fully consistent with the above viewpoint is based on *internal variable* modelling and leads to an efficient computational alternative for the corresponding integro-partial differential equation models. In addition, it provides a "molecular" basis for the models (for a comparison of models of viscoelastic damping via hysteretic integrals versus internal variable representations, see [10] and the references therein).

Our group's interest in viscoelasticity in polymeric materials has been motivated by projects in our Industrial Applied Mathematics Program with at least two of our industrial partners: The Lord Corporation and Medacoustics, Inc. The collaborations with polymer scientists and engineers at Lord involved the dynamic modelling of filled rubbers which experimentally exhibit both significant hysteresis and nonlinearity in tensile and shear deformations as depicted in the sample stress-strain curves in Figure 1. The efforts with engineers at Medacoustics used some of the viscoelastic models we have investigated in attempts to understand the propagation of arterial stenosis induced shear waves in composite biotissue in a sensor development and characterization project.

In some of our earlier efforts [7, 12, 13], the models for hysteretic damping in elastomers employed a phenomenological Boltzmann-type constitutive law of the form

$$\sigma(t) = g_e(\epsilon(t)) + C_D\dot{\epsilon}(t) + \int_{-\infty}^{t} Y(t-s)\frac{d}{ds}g_v\left(\epsilon(s), \dot{\epsilon}(s)\right) ds, \qquad (1)$$

where ϵ is the infinitesimal strain, Y is the convolution memory kernel, and g_e and g_v are nonlinear functions accounting for the elastic and viscoelastic responses of the elastomers, respectively. As explained in [8, 12], our nonlinear materials undergoing large deformations required the use of *finite* (as opposed to *infinitesimal*) strain theories [31]. However, since the nonlinearity between the stress and finite strain is an unknown to be estimated (using

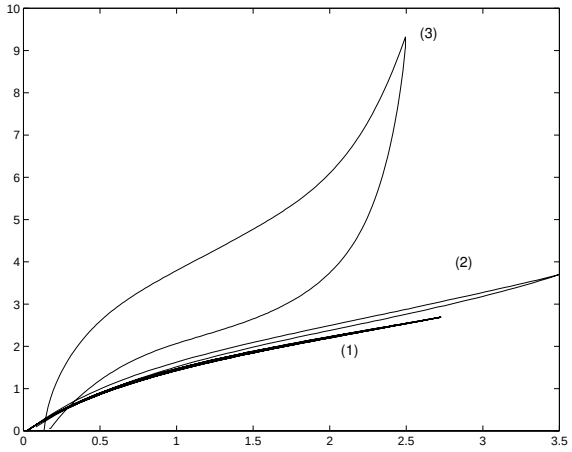

Figure 1: Experimental stress-strain curves for (1) unfilled, (2) lightly filled and (3) highly filled rubber in tensile deformations.

inverse problem algorithms) and since the finite strain can be expressed in terms of known nonlinearities as a function of the infinitesimal strain (at least in the problems we consider), one can effectively formulate the problem as one of estimating the unknown nonlinearity between stress and infinitesimal strain (see [12]). Hence one can develop models for stress in terms of infinitesimal strain. Our previous efforts as summarized in [8] have shown, through comparison with experimental data, that the best fit to filled elastomer data occurs when g_e and g_v are cubic, along with Y as a *distribution* of decaying exponentials. We [3, 9] subsequently developed nonlinear models based on stick-slip "molecular" ideas of Johnson and Stacer [23] and Doi and Edwards [16] which resulted in a form for g_e, g_v and Y that matched the empirical findings reported in [8, 12, 13]. These models allow for multiple relaxation times present in polymer strands of composite materials within a virtual compartmental model of entangled chemically cross-linked/physically constrained system of long chain "molecules". While accounting for multiple relaxation parameters, these models do not include physically or chemically based parameters in representations of the polymer strands.

In the space permitted here, we summarize two recent advances: (i) a new constitutive model [4] that has been developed which combines the virtual stick-slip continuum "molecular-based" ideas of Johnson and Stacer [23] with the Rouse bead chain ideas as described in Doi and Edwards [16]; (ii) a two

dimensional version [5, 27] of a model that accounts for stenosis driven shear wave propagation in biotissue.

The new molecular-based constitutive model, in which polymer chains are treated as Rouse type strings of interconnected beads (a reasonable approximation for many materials), permits the incorporation of many important physical parameters (such as temperature, segment bond length, internal friction, and segment density) in the overall hysteretic constitutive relationship. Its form is similar to that developed in [8, 9] and does have the general form (1) of Boltzmann type, even though the kernel is *not* of convolution type.

In the discussions of the second part of this paper we employ an internal variable formulation of Boltzmann type hysteresis laws to investigate the propagation of stenosis generated waves in biotissue. It is demonstrated that a viscoelastic (as opposed to an elastic) formulation is important and that waves generated in a two-dimensional cylindrical geometry with inner radius partial occlusions can be readily modelled and simulated.

2 A Stick-Slip/Rouse Hybrid Model

We give a brief outline of the new constitutive model; complete details of the derivation can be found in the report [4]. We model a polymer material undergoing directional deformation by assuming it is composed of two *virtual* compartments as depicted in Figure 2. One compartment consists of a *constraining tube* which is a macroscopic compartment containing both CC (chemically cross-linked) and PC (physically constrained) molecules. The other compartment is microscopic in nature and consist of those PC molecules aligned with the direction of the deformation. These molecules will at first "stick" to the constraining tube and be carried along with its motion, but will very quickly "slip" and begin to "relax" back to a configuration of lower strain energy. We compute the contributions of both "compartments" to the overall stress of this polymer material undergoing deformations.

To accomplish this we must consider the contribution from the constraining tube composed of both non-aligned physically constrained molecules and chemically cross-linked molecules, and that of PC molecules aligned in the direction of the deformation that are initially entangled with molecules of the tube. These aligned molecules will in time escape entanglement and become "free" molecules and will thus contribute to the overall stress in two distinct phases: when entrapped and after "leaking" free. Therefore, there

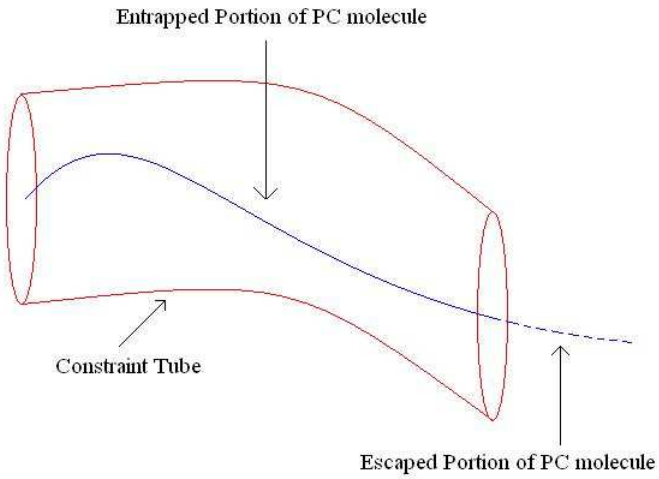

Figure 2: PC molecule entrapped by the surrounding constraining tube.

are three contributions to the stress of the system $\sigma^{(P)}_{\alpha\beta}(t)$: the PC chain in entanglement, the portion of the PC chain that has escaped entanglement and the contribution due to the constraining tube. The constraining tube is treated as elastic while we use the Rouse formulation [16] to treat the aligned PC molecules. We denote the stress of the portion of the polymer chain that is constrained by the surrounding molecules as $\sigma^{(1)}_{\alpha\beta}(t)$, and the stress of the portion of the polymer chain that has leaked out of the constraint tube as $\sigma^{(2)}_{\alpha\beta}(t)$. The total stress contribution of the entangled PC molecules is thus

$$\sigma^{(ve)}_{\alpha\beta}(t) = \sigma^{(1)}_{\alpha\beta}(t) + \sigma^{(2)}_{\alpha\beta}(t).$$

We denote the stress of the constraining tube, assumed to be elastic, by $\sigma^{(elas)}_{\alpha\beta}$. Thus the total polymer dependent stress is given by

$$\sigma^{(P)}_{\alpha\beta}(t) = \sigma^{(ve)}_{\alpha\beta}(t) + \sigma^{(elas)}_{\alpha\beta}(t). \tag{2}$$

Since we assume that the entangled portion of the PC molecule behaves as a free molecule immediately after a deformation, we will use a particular

form of the Rouse model [16] (a free molecular model)

$$\langle X_p^\alpha(t) X_p^\beta(t)\rangle = B_{\alpha\beta}(\mathbf{E}(0)))\frac{\mu_p^2}{2\zeta k_p}e^{-2\xi_p t} + \frac{\mu_p^2}{2\zeta k_p}\delta_{\alpha\beta}\left(1 - e^{-2\xi_p t}\right) \qquad (3)$$

in conjunction with a step-strain process (similar to the stick-slip molecular formulation of Johnson and Stacer [23]) to arrive at an appropriate form for $\sigma_{\alpha\beta}^{(ve)}(t)$, the hysteretic term in a Boltzmann-type stress-strain law. We note that Rouse's model is based on the assumption that the molecule is composed of a continuum limit of a finite number of "beads" connected by some spring-like material (see Figure 3). In (3) ζ is the frictional constant, and μ_p, k_p and ξ_p are constants depending on the Boltzmann's constant k_B, the temperature T, the bond length b and the number N of beads per chain length (or chain length N in the continuum limit). Here $B_{\alpha\beta}(\mathbf{E})$ is the finger strain given in terms of the configuration gradient $\mathbf{E}$. The term $X_p^\alpha(t)$ in Rouse's model represents the α^{th} direction of the p^{th} time dependent Fourier coefficient for the n^{th} bead (or at location n along the chain in the continuum limit) at time t. To calculate the contribution of the entangled portion of

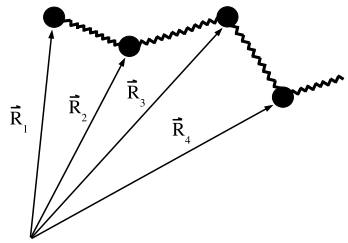

Figure 3: Representation of vectors for a bead-spring polymer molecule.

the molecule to the stress we subject the molecule to a series of step-strains at times $0 = t_0, t_1, \ldots, t_n$, with the additional assumption that during this process some of the entrapped molecule will "leak" and escape entrapment. This "leaked" portion of the molecule will then be considered free, so we therefore assume the Rouse-like expression (3) describes its motion. Then we let the time between each succeeding step-strain go to zero in order to obtain a stress-strain law that describes each node's contribution to the stress after a step-strain is applied to the molecule.

If a tensile deformation is performed on the elastomer along the z axis then the expression for the constitutive law is given by [4]

$$\begin{aligned}
\Sigma_z(t) &= \sigma_{zz}^{(P)}(t) + P \\
&= \sigma_{zz}^{(P)}(t) - \sigma_{xx}^{(P)}(t) \\
&= \sigma_{zz}^{(ve)}(t) - \sigma_{xx}^{(ve)}(t) + \sigma_{zz}^{(elas)}(t) - \sigma_{xx}^{(elas)}(t) \\
&= \sigma_{zz}^{(1)}(t) - \sigma_{xx}^{(1)}(t) + \sigma_{zz}^{(2)}(t) - \sigma_{xx}^{(2)}(t) + \sigma_{zz}^{(elas)}(t) - \sigma_{xx}^{(elas)}(t) \\
&= \frac{6ck_BT}{\pi^2} \sum_{p=1}^{\infty} \left(\frac{1}{p^2} \int_0^t \gamma^3(s) e^{-\frac{2p^2}{\tau_R}(t-s)} \left[2\lambda(s)\lambda'(s) + \frac{\lambda'(s)}{\lambda^2(s)} \right] ds \right. \\
&\quad \left. + \frac{(1-\gamma(t))^3}{p^2} \left(\lambda^2(0) - \frac{1}{\lambda(0)} \right) e^{\frac{-2p^2}{\tau_R}t} \right) + \mu^Y \left(\lambda^2 - \frac{1}{\lambda} \right), \quad (4)
\end{aligned}$$

where c is the segment density, γ is the portion of the PC molecule still constrained by the tube (γ depends on the tube's diameter a as well as the friction constant ζ and bond length b), τ_R (which depends upon ζ and b) and $\lambda = 1 + \epsilon$ (with ϵ being the tensile strain) denotes the principal stretch which represents the deformed length of a unit cube. The term $\mu^Y \left(\lambda^2 - \frac{1}{\lambda}\right)$ accounts for the stress contribution of the elastic tube [6] where μ^Y is the Young's modulus of elasticity. As we mentioned earlier, the integrand in (4) is of the form

$$Y(t,s) \frac{d}{ds} \left(B_{\alpha\beta}(E(s)) \right) = Y(t,s) \frac{d}{ds} \left(\lambda^2(s) - \frac{1}{\lambda(s)} \right),$$

where Y is not of convolution type because of the factor γ. Note that all the parameters in (4) have physical significance attached to them.

2.1 Experimental Validation

To examine and validate the model, we attempted [4] to fit it to several sets of experimental data. One of these, obtained from the experiments conducted by Huang, et al., [25], involved applying a tensile strain to a sample of articular cartilage and then finding the stress within the cartilage. This data set was used to calibrate and validate (4). The strain used in the experiment is a ramp strain; the strain increases at constant rate until a cessation time (t_s). The experimenters then levelled off the strain to a fixed proportion, ϵ_{max}, until the experiment terminates at time $t_f = 2000$

seconds. For the experiment, ϵ_{max} was taken to be 0.05, with a cessation time of $t_s = 400$ seconds. Thus the equation for the strain function is given by

$$\epsilon(t) = \begin{cases} \frac{\epsilon_{max}}{t_s} t & t \leq t_s \\ \epsilon_{max} & t > t_s \end{cases} . \tag{5}$$

We utilized the Matlab tool *Grabit* [20] to extract data from Figure 7 in [25], which is denoted here by y_d. The data extracted was used to estimate the composite parameters $\vec{\theta} = (\tilde{a}, \tilde{b}, c, \tilde{\mu}^Y)^T$ as defined below in (7) (we set T to be 300 K and N to be 1000) using a least-squares criterion

$$C(\vec{\theta}) = \sum_{j=1}^{100} \left| \Sigma_z(t_j; \tilde{a}, \tilde{b}, c, \tilde{\mu}^Y) - y_d \right|^2 . \tag{6}$$

A Nelder-Mead (direct search) method (built into the MatLab function *fminsearch*) will be used to determines the optimal values for the unknown parameters. After an appropriate initial condition is chosen, the optimal value returned by the MatLab program is

$$\vec{\theta}_{opt} = \begin{bmatrix} \tilde{a} \\ \tilde{b} \\ c \\ \tilde{\mu}^Y \end{bmatrix} \equiv \begin{bmatrix} b^4\zeta/a^2 \\ b^2\zeta \\ c \\ \mu^Y/c \end{bmatrix} = \begin{bmatrix} 3.695 \times 10^{-4} \\ 4.0242 \times 10^{-2} \\ 4.6266 \\ 1.9261 \times 10^2 \end{bmatrix} \tag{7}$$

where $\tilde{a}$, $\tilde{b}$ and $\tilde{\mu}^Y$ are defined to remove products of parameters in the optimization. If these parameter values are used in (3), then a very satisfactory (as confirmed by the statistical analysis in [4]) fit of the model to the data is obtained as depicted in Figure 4.

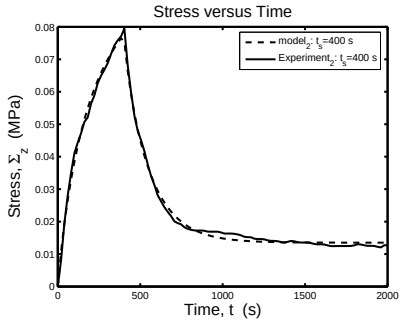

Figure 4: Stress calculation and comparative data for cartilage simulation with ramp strain.

3 Stenosis-Driven Shear Wave Propagation in Biotissue

In this section, we turn to recent results on the viscoelastic models for propagation of stenosis-driven biotissue waves mentioned in the Introduction. Specifically we report on two dimensional models that employ an internal variable approach to model wave propagation. To motivate this, we recall [2] that coronary artery disease (CAD) is caused by atherosclerosis, the gradual accumulation of plaque along the walls of an artery. This buildup, known as a stenosis, restricts the flow of blood, leading to a decrease in the oxygen supply to the heart muscle. It is well known that arterial stenoses produce sounds due to turbulent blood flow in partially occluded arteries. In principle, turbulent normal wall forces exist at and downstream from an arterial stenosis, exerting pressure on the wall of the artery which then causes a small displacement in the surrounding body tissue. Our goal is to model the propagation of the wave generated from the stenosis to the chest wall, and ultimately, to create an inverse problem methodology which can be utilized to determine the location of an arterial stenosis. Here we will compare the viscoelastic model to an elastic one as well as present typical simulations for a biologically motivated example.

The simplified physical geometry which we consider, which is based on physical experiments at Medacoustics, is a cylindrical gel mold as depicted in Figure 5. The synthetic gel of which the cylindrical geometry is comprised has

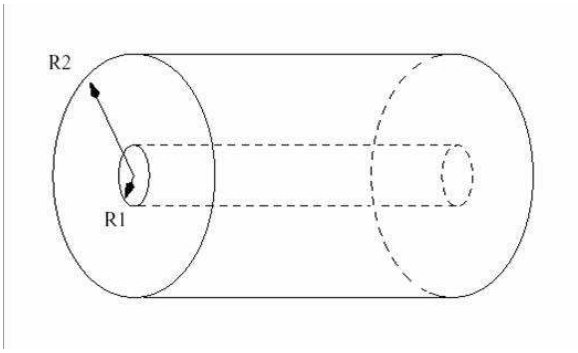

Figure 5: Illustration of the physical geometry considered in our modelling efforts.

material properties similar to those of soft biological tissues. A surgical tube which mimics an artery with stenosis passes axisymmetrically through the center of the mold. A source disturbance (representative of the disturbance caused by stenosis) is generated within the tube. Shear waves propagate through the gel, and acceleration is measured (by sensors) at the outer surface of the gel. The following system of equations were derived from first principles in [27] for this physical geometry:

$$\rho\frac{\partial^2 u_1}{\partial t^2} = \frac{\partial}{\partial r}(\epsilon_\lambda + \epsilon_\mu^{11}) + \frac{1}{r}\frac{\partial}{\partial\theta}(\epsilon_\mu^{21}) + \frac{1}{r}(\epsilon_\mu^{11} - \epsilon_\mu^{22}) \tag{8}$$

$$\rho\frac{\partial^2 u_2}{\partial t^2} = \frac{\partial}{\partial r}(\epsilon_\mu^{12}) + \frac{1}{r}\frac{\partial}{\partial\theta}(\epsilon_\lambda + \epsilon_\mu^{22}) + \frac{1}{r}(\epsilon_\mu^{12} + \epsilon_\mu^{21}) \tag{9}$$

$$\frac{\partial\epsilon_{\lambda_k}}{\partial t} = -\nu_{\lambda_k}\epsilon_{\lambda_k} + C_{\lambda_k}\frac{\partial}{\partial t}\left(S_{11}^{(e)} + S_{22}^{(e)}\right) \tag{10}$$

$$\frac{\partial\epsilon_{\mu_k}^{11}}{\partial t} = -\nu_{\mu_k}\epsilon_{\mu_k}^{11} + C_{\mu_k}\frac{\partial}{\partial t}\left(S_{11}^{(e)}\right) \tag{11}$$

$$\frac{\partial\epsilon_{\mu_k}^{12}}{\partial t} = -\nu_{\mu_k}\epsilon_{\mu_k}^{12} + C_{\mu_k}\frac{\partial}{\partial t}\left(S_{12}^{(e)}\right) \tag{12}$$

$$\frac{\partial\epsilon_{\mu_k}^{22}}{\partial t} = -\nu_{\mu_k}\epsilon_{\mu_k}^{22} + C_{\mu_k}\frac{\partial}{\partial t}\left(S_{22}^{(e)}\right), \quad k = 1, 2, \ldots, K, \tag{13}$$

where u_1 and u_2 are displacement in the radial and tangential directions, respectively, ϵ_{λ_k} and $\epsilon_{\mu_k}^{ij}$ represent the K internal variables, ν_i and C_i are material parameters. The $S_{ij}^{(e)}$ represent the elastic response, given by the equations

$$\begin{aligned}
S_{11}^{(e)} = \frac{\partial\rho_0 W^{(2)}}{\partial E_{11}} &= 2(\alpha_1 E_{11} + \alpha_4 E_{22}) + 2c(a_1 E_{11} + a_4 E_{22})\exp(a_1 E_{11}^2 \\
&\quad + a_2 E_{22}^2 + a_3 E_{12}^2 + a_3 E_{21}^2 + 2a_4 E_{11} E_{22}) \\
S_{12}^{(e)} = \frac{\partial\rho_0 W^{(2)}}{\partial E_{12}} &= 2\alpha_3 E_{12} + 2ca_3 E_{12}\exp(a_1 E_{11}^2 + a_2 E_{22}^2 + a_3 E_{12}^2 \\
&\quad + a_3 E_{21}^2 + 2a_4 E_{11} E_{22}) \\
S_{22}^{(e)} = \frac{\partial\rho_0 W^{(2)}}{\partial E_{22}} &= 2(\alpha_4 E_{11} + \alpha_2 E_{22}) + 2c(a_4 E_{11} + a_2 E_{22})\exp(a_1 E_{11}^2 \\
&\quad + a_2 E_{22}^2 + a_3 E_{12}^2 + a_3 E_{21}^2 + 2a_4 E_{11} E_{22}).
\end{aligned}$$

Several different variations of the elastic response were considered in [27]. For the first elastic response model (ER1), it was assumed that the off diagonal

strain terms, E_{12}, were equal to zero, and that the small stress terms were negligible ($\alpha_i = 0$). The second elastic response model (ER2) was formulated under the assumption that the small stress terms were negligible, while the third elastic response model (ER3) retained the small stress terms and assumed that the off diagonal strain elements were zero. Statistical significance tests were employed to determine which versions of the model produced best fits to radially symmetric (and hence 1-dimensional) data presented in [2]. From this it was determined that the first elastic response model employing two (i.e., $K = 2$) internal variables (denoted by (ER1-2ISV)) provided one of the best fits. Thus, the results presented here were all generated using that model.

Equations (8) and (9) are variations of the equations of motion. They are derived from the physical properties of conservation of mass and conservation of momentum. The remaining equations (10)-(13) represent the dynamics of the k^{th} internal variable. They are based on the internal variable approach employed in [2] as an approximation of and alternative to Fung's quasi-linear viscoelastic theory.

In [19], Fung develops and presents the quasi-linear viscoelastic constitutive equation

$$S_{ij}(t) = \int_{-\infty}^{t} G_{ijkl}(t-\tau)\frac{\partial S_{kl}^{(e)}[\bar{E}(\tau)]}{\partial \tau}d\tau, \tag{14}$$

where S_{ij} is the Kirchoff stress tensor, $\bar{E}$ is the Green's strain tensor, G_{ijkl} is a reduced relaxation function, and $S_{kl}^{(e)}$ is the "elastic" stress tensor.

Since its introduction, this quasi-linear viscoelastic (QLV) theory has been applied successfully in stress-strain experiments to several types of biological tissue. A benefit to using (14) as a constitutive equation is that, unlike simpler models for viscoelasticity, it allows for the consideration of a continuous spectrum (e.g., see the discussions in [19]) of relaxation times and frequencies (this is also true of the probabilistic-based internal variable approach we developed in [11]). While Fung's theory has been successfully employed for fitting hysteretic stress-strain curves, we are interested in using it in a full dynamical model. Unfortunately, the QLV, as presented by Fung, leads to exceedingly difficult computations within full dynamical partial differential equations, especially in inverse problems. This motivated the development of the internal variable approach described in [2, 11, 27] (which permits discrete approximation to a continuum) in attempts to approximate well the corresponding dynamic responses even in cases where the stress-strain curves alone

do not produce adequate approximations – see [19] for discussions.

Our alternative to Fung's kernel is a parameter dependent kernel with a continuous distribution of parameters and internal variables. In the case of a finite combination of Dirac δ distributions (employed in this presentation), we obtain a finite summation of exponential functions as our approximation kernel. This method can be extended to allow for consideration of a continuous spectrum of relaxation times and frequencies by utilizing absolutely continuous parameter distributions in place of the δ distributions.

To numerically integrate our system, we first used a series of substitutions so that we could rewrite it as a system of first order partial differential equations for a vector U containing velocities v_i and strains w_i. We utilized the MacCormack finite difference scheme (see [33]) to numerically integrate the system. This scheme is a two-step method with second order accuracy which uses forward differences on the first step, followed by a step of backward differences.

To update boundary terms, we used direction cosines (see, e.g., [24]). If the characteristic curve points into the domain, then a physical boundary condition is prescribed for the boundary. Otherwise, the boundary values are updated utilizing the second order discretization

$$U^{n+1} = U^n + \Delta t[AU_r + BU_\theta + Q]^n + \frac{1}{2}\Delta t^2[AU_r + BU_\theta + Q]_t^n. \qquad (15)$$

As there is only one characteristic pointing into the domain at both the inner and outer radius, we prescribed the following boundary conditions. On the inner radius, $w_1(R_1, \theta, t) = f(t)$, where $f(t)$ is an approximate impulse input function similar to that used in [2]. On the outer radius, we prescribe $w_1 = 0$.

Although our models (and those of Fung) have been derived under the widely accepted assumption that biotissue has viscoelastic properties, there are other groups [21, 22, 29] conducting research in this field that utilize non-dissipative constitutive equations related to elastic media for their modelling efforts. This raises the question as to whether the more complicated viscoelastic models, as proposed by Fung, our group and others, really are required. We therefore examined the difference between a model employing an elastic assumption and one which assumes viscoelasticity as formulated here. The Maxwell, Voigt, and Kelvin models for viscoelasticity are rather easily reduced to an elastic model by setting the viscous portion to be zero. In a similar manner we can easily reduce our model to a purely elastic model, and thus the models are readily compared.

By considering a summation of exponential functions to approximate the Fung kernel, we defined

$$\lambda(t) = C_\lambda e^{-\nu_\lambda t}; \quad \mu(t) = C_\mu e^{-\nu_\mu t}.$$

As detailed in [27], if we allow the relaxation parameters ν_λ and ν_μ to tend towards zero, then our model reduces to a purely elastic model. To examine the effect of the ν parameters on our system, we ran simulations with values of $10\nu_k^*, \nu_k^*, \frac{\nu_k^*}{10}, \frac{\nu_k^*}{50}$, and $\nu_k = 0$, where ν_k^* represents the optimized parameter from [27] using the radially symmetric data.

All simulations and boundary conditions were treated as explained previously. Figure 6 depicts time snapshot results for v_1 for different values of ν at two different time steps.

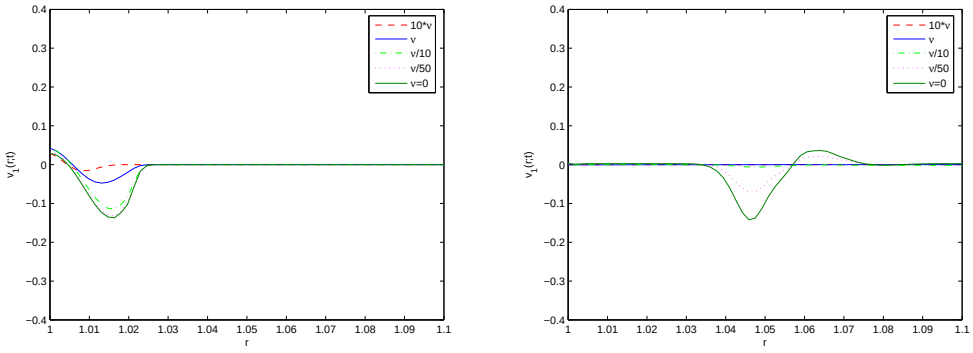

Figure 6: Results for v_1 for the varying values of the relaxation parameter, ν at t=0.0032 (left) and t=0.0504 (right).

We observe from Figure 6 that as time increases, the solutions produced using larger values for the relaxation parameter exhibit more dissipation. By time $t = 0.0504$ seconds (depicted in Figure 6 (right)), it is evident that the only wave which has shown no dissipation is that which was generated using the purely elastic model (i.e., $\nu = 0$). This is what one would expect from a wave travelling in a purely elastic medium. The wave should simply reflect from one boundary to the other, travelling back and forth with no dissipation (which we note does NOT agree with behavior in any biotissue material). Our results illustrate that setting $\nu = 0$ effectively reduces our model from viscoelastic to elastic in nature.

While our results demonstrate that our model can be easily reduced to an elastic model, they also indicate that the results produced by an elastic model vary significantly from the results generated by a model incorporating viscoelasticity. Since we know dissipation occurs in biotissue, this supports the argument that the viscoelastic model clearly is a more realistic model. The difference between the elastic and viscoelastic simulations motivate our efforts in using a viscoelastic approach to modelling wave propagation in biotissue.

Having numerically motivated the use of a viscoelastic model, we next present simulation results generated by the model for a geometry modified to represent a stenosis. We assumed that a buildup of plaque (cholesterol, calcium, and platelets) has formed along the wall of the inner radius of our geometry (see Figure 7). We assumed that this buildup is completely rigid and impermeable, thus any impulse along the inner radius will have no direct effect on the region occluded by the buildup.

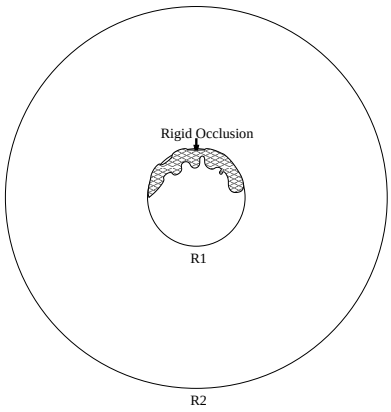

Figure 7: Geometry with occlusion along inner radius.

In order to numerically solve our system under these conditions, we shall define the impulse along the inner radius as follows: $w_1(t; R_1, \theta) = f_1(t) * s(\theta)$, where $f_1(t)$ is the impulse function used above and $s(\theta)$ is defined as the characteristic function for $[0, \theta_1) \cup (\theta_2, 2\pi]$. For the computational simulations presented here, we assumed that the occlusion occupied the area between $\theta_1 = \frac{3\pi}{8}$ and $\theta_2 = \frac{5\pi}{8}$. Computations were again carried out using the MacCormack scheme, and boundary values were again updated using direction cosines. However, the input function, $w_1(t; R_1, \theta)$, as defined above,

now has discontinuities at the edges of the occlusion (θ_1 and θ_2). These discontinuities present numerical difficulties with the integration scheme, and must be treated with certain precautions [24, 26]. Although the method of direction cosines permits one to prescribe only one boundary condition (corresponding to the one eigendirection that points into the domain) on the inner radius, the presence of discontinuities in the input permits the assignment of additional conditions. To ensure that the problem is well defined, we must define the velocity across the discontinuity. Hirsch [24] argues that in this situation, one should define the tangential velocity to be zero across the discontinuity. This means that we may prescribe $v_2(t; 0, \theta_1 \pm \epsilon) = 0$ and $v_2(t; 0, \theta_2 \pm \epsilon) = 0$. We ran our simulations using the discontinuous inner radius boundary conditions, as well as the new boundary conditions; typical results are displayed in Figures 8 and 9.

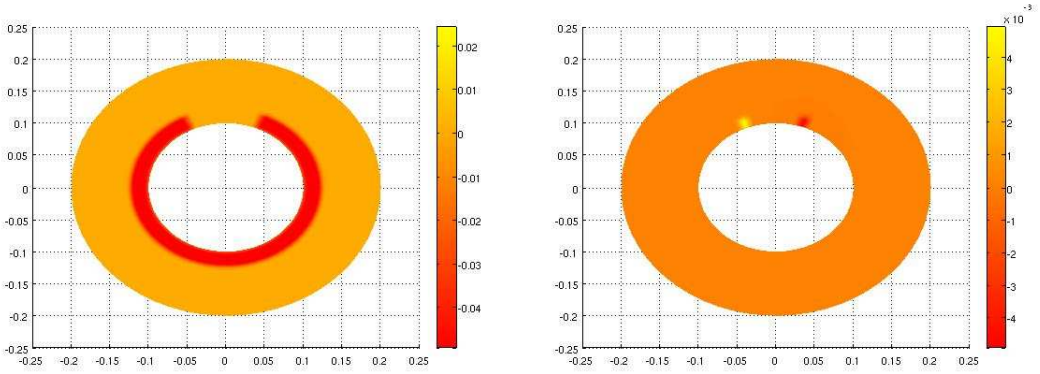

Figure 8: Results for v_1 (left) and v_2 (right) for the geometry with an occluded inner radius, t=0.0039.

By examining Figures 8 and 9, we observe that as time increases, the radial velocity (depicted by the graphs on the left of each figure) propagates outward uniformly throughout the geometry, with the exception of the area affected by the occlusion. The tangential velocity is also propagating outward, but this only occurs around the interface between the occluded and non-occluded portion of the inner radius.

The results summarized here and further detailed in [5, 27] illustrate an ability to simulate stenosis-driven wave propagation through homogeneous

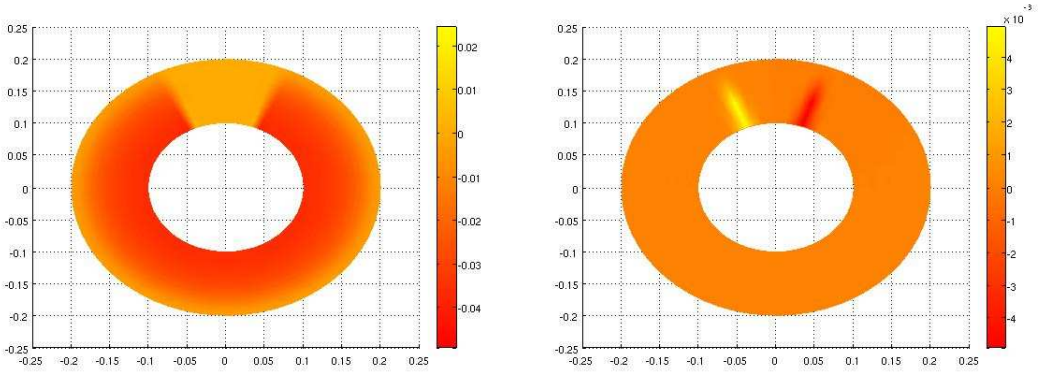

Figure 9: Results for v_1 (left) and v_2 (right) for the geometry with an occluded inner radius, t=0.0162.

biotissue. Of course, the composition of the human chest cavity is much more complex than the geometry considered in the model presented here. The inclusion of heterogeneities due to different tissues (lung, bone, etc.) present in the chest cavity is necessary for improvement of our modelling efforts. (Initial results in this direction are presented in [5, 27].) Nevertheless, this model and its simulation capabilities provide a solid foundation for the inclusion of heterogeneities, as well as a good starting point for examining inverse problems formulated to determine the location and extent of a stenosis within a given two or three dimensional geometry.

Acknowledgements

This research was supported in part by the US Air Force Office of Scientific Research under grant AFOSR-FA9550-04-1-0220. It was also supported in part by a GAANN Fellowship to JRS under grant U.S. Department of Education P200A030277 and in part by The David and Lucile Packard Foundation by a Packard Fellowship to NSL.

References

[1] I.Babuska, K. Jerina, Y. Li and P.Smith, Quantitative assessment of the accuracy of constitutive laws for plasticity with an emphasis on cyclic deformation, in *Material Parameter Estimation for Modern Constitutive Equations,*, (L.A. Bertram, S.B. Brown and A.D. Freed, eds.), Proc. 1993 ASME Winter Annual Meeting, New Orleans, Louisiana, MD-Vol.**43**/AMD-Vol.**168**, ASME, New York, 1993, pp. 113–169.

[2] H.T. Banks, J.H. Barnes, A. Eberhardt, H. Tran and S. Wynne, Modeling and computation of propagating waves from coronary stenoses, *Computational and Applied Mathematics*, **21** (2002), 767–788.

[3] H.T. Banks, J.B. Hood and N.G. Medhin, A molecular based model for polymer viscoelasticity: Intra- and inter-molecular variability, Technical Report CRSC-TR04-39, NCSU, December, 2004; *Applied Mathematical Modelling*, submitted.

[4] H.T. Banks, J.B. Hood, N.G. Medhin and J.R. Samuels, A stick-slip/Rouse hybrid model for viscoelasticity in polymers, Technical Report CRSC-TR06-26, NCSU, November, 2006; *Nonlinear Analysis: Real World Applications*, submitted.

[5] H.T. Banks and N.S. Luke, Simulations of propagating shear waves in biotissue employing an internal variable approach to dissipation, Technical Report CRSC-TR06-28, NCSU, December, 2006.

[6] H.T. Banks and Nancy Lybeck, Modeling methodology for elastomer dynamics, Technical Report CRSC-TR96-29, NCSU, September, 1996.

[7] H.T. Banks, N.J. Lybeck, M.J. Gaitens, B.C. Muñoz and L.C. Yanyo, Modeling the dynamic mechanical behavior of elastomers, Technical Report CRSC-TR96-26, NCSU, September, 1996.

[8] H.T. Banks, N.G. Medhin and G.A. Pinter, Multiscale considerations in modeling of nonlinear elastomers, Technical Report CRSC-TR03-42, NCSU, October, 2003; *J. Comp. Meth. Sci. and Engr.*, to appear.

[9] H.T. Banks, N.G. Medhin and G.A. Pinter, Nonlinear reptation in molecular based hysteresis models for polymers, *Quarterly Applied Math.*, **62** (2004), 767–779.

[10] H.T. Banks and G.A. Pinter, Damping: hysteretic damping and models, CRSC-TR99-36, NCSU, December, 1999; in *Encyclopedia of Vibration*, (S.G. Braun, D. Ewins and S. Rao, eds.), Academic Press, London, 2001, pp. 658-664.

[11] H.T. Banks and G.A. Pinter, A probabilistic multiscale approach to hysteresis in shear wave propagation in biotissue, *Multiscale Modeling and Simulation*, **3** (2005), 395–412.

[12] H.T. Banks, G.A. Pinter, L.K. Potter, M.J. Gaitens and L.C. Yanyo, Modeling of quasi-static and dynamic load responses of filled viscoelastic materials, Technical Report CRSC-TR98-48, NCSU, December, 1998; Chapter 11 in *Mathematical Modeling: Case Studies from Industry* (E. Cumberbatch and A. Fitt, eds.), Cambridge University Press, 2001, pp. 229-252.

[13] H.T. Banks, G.A. Pinter, L.K. Potter, B.C. Muñoz and L.C. Yanyo, Estimation and control related issues in smart material structures and fluids, Technical Report CRSC-TR98-02, NCSU, January, 1998; *Optimization Techniques and Applications* (L. Caccetta, et al., eds.), Curtain Univ. Press, July, 1998, pp. 19-34.

[14] H.T. Banks, H.T. Tran and S. Wynne, A well-posedness result for a shear wave propagation model, Technical Report CRSC-TR01-31, NCSU, Dec. 2001; *Proceedings 8th Int'l Conference on Control of DPS* (July, 2001, Graz, Austria), *Int'l Series of Num. Math*, Vol. 143, Birkhauser Verlag, Basel, 2002, pp. 25-40.

[15] M. Doi, *Introduction to Polymer Physics*, Clarendon Press, Oxford, 1996.

[16] M. Doi and S.F. Edwards, *The Theory of Polymer Dynamics*, Oxford, New York, 1986.

[17] J.D. Ferry, *Viscoelastic Properties of Polymers*, John Wiley and Sons, Inc., New York, 1961.

[18] Y.C. Fung, *Foundations of Solid Mechanics*, Prentice-Hall, Englewood Cliffs, NJ, 1965.

[19] Y.C. Fung, *Biomechanics: Mechanical Properties of Living Tissues*, Springer-Verlag, New York, 1993.

[20] Jiro Doke, *Grabit.m*, *The MathWorks MatLab Central Website*, March 17, 2005, http://www.mathworks.com/matlabcentral/fileexchange (accessed April 13, 2005).

[21] L. Ji and J. McLaughlin, Recovery of the Lamé parameter μ in biological tissues, *Inverse Problems*, **20** (2004), 1–24.

[22] L. Ji, J. McLaughlin, D. Renzi and J-R Yoon, Interior elastodynamics inverse problems: shear wave speed reconstruction in transient elastography, *Inverse Problems*, **19** (2003), S1–S29.

[23] A.R. Johnson and R.G. Stacer, Rubber viscoelasticity using the physically constrained system's stretches as internal variables, *Rubber Chemistry and Technology*, **66** (1993), 567–577.

[24] C. Hirsch, *Numerical Computation of Internal and External Flows, Volume 2*, John Wiley & Sons, Chichester, England, 1990.

[25] C.Y. Huang, V.C. Mow and G.A. Ateshian, The role of flow-independent viscoelasticity in the biphasic tensile and compressive responses of articular cartilage, *J. Biomech. Eng.*, **123** (2001), 410–417.

[26] A.G. Kulikovskii, N.V. Pogorelov and A.Y. Semenov, *Mathematical Aspects of Numerical Solution of Hyperbolic Systems*, Chapman & Hall/CRC Press, Boca Raton, Florida, 2001.

[27] N.S. Luke, *Modeling Shear Wave Propagation in Biotissue: An Internal Variable Approach to Dissipation*, Ph.D. dissertation, NC State University, August, 2006.

[28] J.E. Marsden and T.J.R. Hughes, *Mathematical Foundations of Elasticity*, Prentice-Hall, Englewood Cliffs, NJ, 1983.

[29] J.R. McLaughlin and J-R Yoon, Unique identifiability of elastic parameters from time-dependent interior displacement measurement, *Inverse Problems*, **20** (2004), 25–45.

[30] R.W. Ogden, *Non-Linear Elastic Deformations*, Ellis Horwood Limited, Chichester, 1984.

[31] R.S. Rivlin, Large elastic deformations of isotropic materials, I, II, III, *Phil. Trans. Roy. Soc. A* **240** (1948), 459-525.

[32] J.K. Stille, *Introduction to Polymer Chemistry*, John Wiley and Sons, Inc., New York, 1962.

[33] J.C. Strickwerda, *Finite Difference Schemes and Partial Differential Equations*, Wadsworth, Inc., California, 1989.

[34] L.R.G. Treloar, *The Physics of Rubber Elasticity*, Clarendon, Oxford 1975.

[35] I.M. Ward, *Mechanical Properties of Solid Polymers*, J. Wiley & Sons, New York, 1983.